Available online at www.sciencedirect.com
SCIENCE DIRECT®
International Journal of Heat and Mass Transfer 47 (2004) 853–864
International Journal of HEAT and MASS TRANSFER
www.elsevier.com/locate/ijhmt

Benchmark solutions for natural convection in a cubic cavity using the high-order time–space method

Shinichiro Wakashima *, Takeo S. Saitoh

School of Environmental Studies, Tohoku University, Sendai 980-8579, Japan

Received 17 January 2003

Abstract

Benchmark numerical solutions for a three-dimensional natural convection heat transfer problem in a cubical cavity are presented in this paper. The 3-D cavity has two differentially heated and isothermal vertical walls and also four adiabatic walls. The computations are conducted for three Rayleigh numbers of 10^4, 10^5 and 10^6. The filled fluid is with air and the Prandtl number is fixed at 0.71. The computed results are efficiently obtained by using the time–space method, which was proposed by Saitoh (1991) as a highly efficient and fast solver for general heat transfer and fluid flow problems. In our computations, the high-accuracy finite differences of a fourth-order were employed for the spatial discretization of governing equations and boundary conditions. In addition the third-order backward finite difference was used in timewise discretization. The resultant converged flow and temperature characteristics are also presented. The spatial grid dependency of the solutions was examined on a uniform grid. In addition, the grid-independent benchmark solutions were obtained by Richardson extrapolation for three cases. The present benchmark solutions will be useful for checking the performance and accuracy of any numerical methodologies.

1. Introduction

A lot of numerical experiments for a natural-convection-dominated heat transfer problem have been conducted. Particularly, many experiments for natural convections in an enclosure were performed motivated from the wide variety of engineering applications, i.e., crystal growth, metal casting and phase change such as freezing of water for latent heat thermal storage systems. Some of such numerical experiments became to be known as the benchmark solutions (BMSs), which would be used for the investigation of performance of numerical methodologies solving the incompressible Navier–Stokes equations and the comparison to each other.

One of the most popular benchmark problems is that of laminar flow in a two-dimensional square cavity with differentially heated sidewalls. At first, de Vahl Davis proposed the laminar regime benchmarks for the Rayleigh numbers up to 10^6 using the second-order centered finite difference scheme [1]. Later, the benchmark solution with the fourth-order of accuracy was given by Saitoh and Hirose [2] for Rayleigh number of 10^4. They also had verified the stable computations for higher Rayleigh numbers up to 10^8. Hortmann et al. [3] have proposed the benchmark solutions for Rayleigh numbers up to 10^6 using the multi-grid finite volume method on 640×640 non-uniform high-resolution grids.

These computations are mainly conducted in two-dimensions. Naturally, an extension of this BMS to the three-dimensions has been considered. Mallinson and de Vahl Davis [4] had already performed the computation up to the Rayleigh number of 10^6 using a coarse grid spacing of only $15\times15\times15$. They also investigated the effect of a certain aspect of a ratio for flow patterns. Le Peutrec and Lauriat [5] investigated the effect of heat losses from conductive sidewalls of a cavity for Rayleigh numbers up to 10^7 using a non-uniform spacing grid of $31\times31\times31$ and $41\times41\times41$. Fusegi et al. [6] calculated

* Corresponding author. Tel./fax: +81-22-217-4067.
E-mail address: swaka@cc.mech.tohoku.ac.jp (S. Wakashima).

0017-9310/$ - see front matter © 2003 Elsevier Ltd. All rights reserved.
doi:10.1016/j.ijheatmasstransfer.2003.08.008

Nomenclature

a	thermal diffusivity
C	some constant value
Gr	Grashof number, $g\beta H^3\Delta T/v^2$
g	acceleration due to gravity
H	height of cavity
Nu	Nusselt number, $PrRe\boldsymbol{u}T - \frac{\partial T}{\partial \boldsymbol{n}}$
$\boldsymbol{n}$	normal vector
Pr	Prandtl number, v/a
Ra	Rayleigh number, $g\beta H^3\Delta T/av$
Re	Reynolds number, $\sqrt{Gr}$
S	stratification factor
T	dimensionless temperature
t	dimensionless time or timewise coordinate
U	reference velocity, $(g\beta H\Delta T)^{1/2}$
u	velocity vector
x, y, z	spatial coordinates
$\hat{\boldsymbol{i}}, \hat{\boldsymbol{j}}, \hat{\boldsymbol{k}}$	unit vectors for the x-, y- and z-directions

Greek symbols

α	acceleration parameter for iterations
β	volumetric expansion coefficient of fluid
ω	vorticity vector
Δ	grid spacing or difference
ϕ	vector potential
v	kinematic viscosity

Subscripts and superscripts

c	cooled (cold)
center	center of cavity
h	heated (hot)
i	x-direction grid point index
j	y-direction grid point index
k	z-direction grid point index
l	t-direction grid point index
local	local value
max	maximum value
mean	mean value
min	minimum value
n	iteration number, normal direction
0	initial value
1/2	mid-plane of cavity
1	x-component
2	y-component
3	z-component
+	dimensional quantities

an air-filled cubical cavity of two cases for the Rayleigh numbers of 10^4 and 10^6 using a QUICK scheme on fine and non-uniform $64\times64\times64$ grids, and clarified three-dimensional structures of flow, vorticity and temperature in the cavity. They also compared their numerical results with the experimental measurements [7]. The results for Rayleigh number of 10^6 and the steady case by Janssen et al. [8] were conducted using the second-order finite volume method on very fine and non-uniform grids of $120\times120\times120$. Although, they made an assumption that flow and temperature distribution is symmetrical, they also employed a zero-gradient pressure boundary condition. Wei et al. [9] had pointed out that such a zero-gradient condition for pressure was not appropriate for a buoyant-dominated flow.

In this paper, the new benchmark solutions having a fourth-order of accuracy for the three-dimensional natural convection problem in a cubical cavity with differentially heated vertical walls present. The computations are conducted throughout the cavity (i.e., without any assumptions of symmetric for the solutions). The governing equations are discretized using the fourth-order in space and the third-order in time finite difference schemes on the uniform spatial grids up to $120\times120\times120$.

In order to obtain the solutions, we used the time–space method (TSM) proposed by Saitoh et al. [10], which can produce a great reduction of CPU time (up to 1/100th–1/1000th) compared with that of the conventional time-marching methods. The TSM has already shown its efficiency for a 2-D melting/freezing problem (Saitoh et al. [11]) and a 2-D high Rayleigh number problem. When the natural convection problems are computed by using the ordinary finite difference and finite volume methods, particularly in cases with a high Rayleigh number, both linear and non-linear instability causes the strict limitation of the time step for continuing stable computations. In addition, thin boundary layers developed near the walls need finer spacing of numerical grids, thereby, requiring an enormous amount of CPU time.

2. Time–space method

The conventional time-marching method integrates step by step in a timewise direction from the initial state, independently from the spatial directions. This often creates severe numerical instability due to non-linearity of the governing equations and/or other instability sources included in the system to be computed. Even if implicit-type methods were employed, the time step should still be very small. This situation requires a great number of time steps and enormous CPU time. The natural convection problems with a high Rayleigh

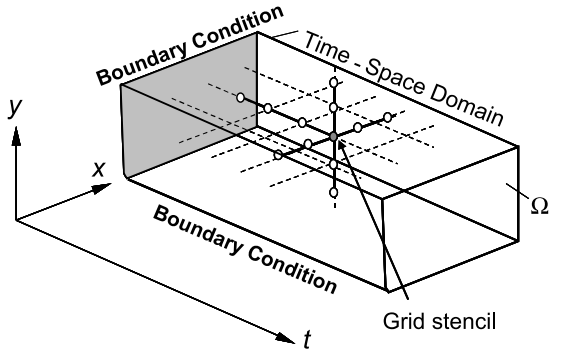

Fig. 1. Conceptual sketch of the TSM and the time–space domain.

number and phase change (moving boundary problems) are typical examples. In these computations, high resolutions within boundary layers or a stable tracking of the moving boundaries are highly required, and an extremely small time step size is needed due to such requirements.

On the other hand, the TSM takes a different approach, i.e., the timewise coordinate is referred to as one of the spatial coordinates, which is included into a time–space coordinate domain. Fig. 1 shows the conceptual sketch of the TSM and the relevant time–space computational domain. In general, the TSM employs an iterative procedure for obtaining whole solutions in the time–space domain. The $\{n\}$-dimensional unsteady boundary-value problem is transformed into the $\{n+1\}$-dimensional steady boundary-value problem, and the initial condition corresponds to the boundary condition at $t=0$ in the TSM calculation. No error propagation or accumulation occurs in the time–space domains. Hence, it is unconditionally stable and the time step is chosen arbitrarily. The time step will be determined only to satisfy the degree of accuracy or the degree of resolution in the timewise direction. The TSM has shown its efficiency for a 2-D melting/freezing problem [11] with high Rayleigh numbers. Here we applied the TSM to the three-dimensional natural convection in a cubical cavity.

3. Numerical model of three-dimensional natural convection heat transfer in a cubic cavity

3.1. The model description and governing equations

The schematic model for the problem is shown in Fig. 2. The cavity has an aspect ratio of unity and is filled with the working fluid of air. The Prandtl number is fixed at 0.71. All surrounding walls are rigid and impermeable. The vertical walls located at $x=0$ and $x=1$ are retained to be isothermal but at different temperatures of T_h and T_c, respectively. The remaining four sidewalls are taken as adiabatic. The buoyancy force due to gravity works downwards (i.e., in negative z-direction) as shown in Fig. 2. In addition, the following assumptions for working fluid are used in the analysis:

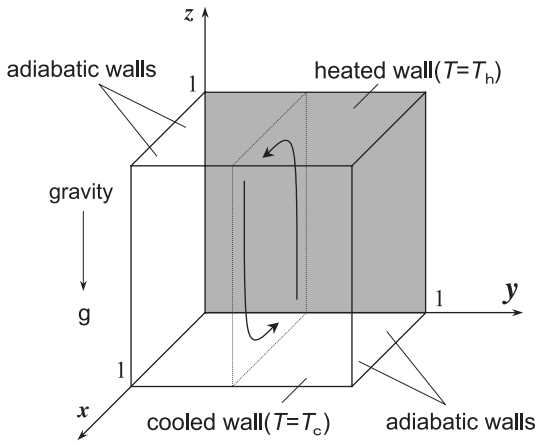

Fig. 2. Schematic model for the natural convection in a cubical cavity.

(1) Flow is incompressible and laminar.
(2) The Boussinesq approximation is valid.

By virtue of the above assumptions, the non-dimensional governing equations, i.e., the momentum equation, energy (temperature) equation and mass conservation equation are transformed into vorticity-vector potential forms. They can be expressed in Cartesian coordinates as follows [4]:

$$\frac{\partial\omega}{\partial t}+(u\cdot\nabla)\omega-(\omega\cdot\nabla)u=\frac{1}{Re}\nabla^2\omega+\frac{Gr}{Re^2}\left[\frac{\partial T}{\partial y},-\frac{\partial T}{\partial x},0\right], \tag{1}$$

$$\frac{\partial T}{\partial t}+(u\cdot\nabla)T=\frac{1}{PrRe}\nabla^2T, \tag{2}$$

$$\nabla^2\phi=-\omega, \tag{3}$$

$$\omega=\nabla\times u, \tag{4}$$

$$u=\nabla\times\phi, \tag{5}$$

where,

$$\nabla=\frac{\partial}{\partial x}\hat{\boldsymbol{i}}+\frac{\partial}{\partial y}\hat{\boldsymbol{j}}+\frac{\partial}{\partial z}\hat{\boldsymbol{k}}.$$

Here, ω is the non-dimensional vorticity vector, u is the non-dimensional velocity vector, T is the non-dimensional temperature and ϕ is the vector potential. Pr is the Prandtl number ($Pr=\nu/a$), Ra is the Rayleigh number ($Ra=g\beta H^3\Delta T/a\nu$), Gr is the Grashof number,

and Re is the Reynolds number. In this paper, those are related as $Gr = Ra/Pr = Re^2$. $\hat{\boldsymbol{i}}$, $\hat{\boldsymbol{j}}$ and $\hat{\boldsymbol{k}}$ are the unit vectors for the x-, y- and z-direction, respectively.

The dimensional quantities were non-dimensionalized as follows:

$$(x,y,z) = (x^+,y^+,z^+)/H, \quad (u_1,u_2,u_3) = (u_1^+,u_2^+,u_3^+)/U,$$
$$t = t^+U/H, \quad T = (T^+ - T_c^+)/(T_h^+ - T_c^+),$$
$$\Delta T = T_h^+ - T_c^+, \quad U = (g\beta H \Delta T)^{1/2},$$

where superscript (+) denotes the dimensional variables, and subscripts (1), (2) and (3) denote the components for the x-, y- and z-directions, respectively.

The boundary conditions are given as follows:

(i) Temperature

$$T = 1 \text{ at } x = 0, \quad T = 0 \text{ at } x = 1,$$
$$\frac{\partial T}{\partial n} = 0 \text{ on other walls.}$$

(ii) Vorticity

$$\omega_1 = 0, \quad \omega_2 = -\frac{\partial u_3}{\partial x}, \quad \omega_3 = \frac{\partial u_2}{\partial x} \text{ at } x = 0 \text{ and } 1,$$
$$\omega_1 = \frac{\partial u_3}{\partial y}, \quad \omega_2 = 0, \quad \omega_3 = -\frac{\partial u_1}{\partial y} \text{ at } y = 0 \text{ and } 1,$$
$$\omega_1 = -\frac{\partial u_2}{\partial z}, \quad \omega_2 = \frac{\partial u_1}{\partial z}, \quad \omega_3 = 0 \text{ at } z = 0 \text{ and } 1.$$

(iii) Vector potential

$$\frac{\partial \phi_1}{\partial x} = \phi_2 = \phi_3 = 0 \text{ at } x = 0 \text{ and } 1,$$
$$\phi_1 = \frac{\partial \phi_2}{\partial y} = \phi_3 = 0 \text{ at } y = 0 \text{ and } 1,$$
$$\phi_1 = \phi_2 = \frac{\partial \phi_3}{\partial z} = 0 \text{ at } z = 0 \text{ and } 1.$$

(iv) Velocity

$$u = 0 \text{ on all walls,}$$

where n indicates the normal vector to the wall surface.

Boundary conditions for vorticity are directly derived from the velocity boundary conditions and the definition of vorticity (i.e., $\omega = \nabla \times u$). The initial conditions of isothermal and being at rest serves as the boundary conditions at $t = 0$ in the time–space domain.

For the initial distributions in the time–space domain, the non-dimensional temperature, non-dimensional velocity vector and non-dimensional vorticity vector at $t = 0$ are simply duplicated to all time levels as follows:

$$T = 1 \text{ at } x = 0, \quad T = 0 \text{ at } x \neq 0,$$
$$u = (0,0,0), \quad \omega = (0,0,0). \tag{6}$$

3.2. Discretization method

All variables are co-located at each grid point. As the spatial discretizations method, the fourth-order centered finite difference (FD) scheme was used for the first and second derivatives in governing equations. For example, those terms are expressed in the x-direction as follows:

$$\left(\frac{\partial \phi}{\partial x}\right)_{i,j,k,l} = \frac{\phi_{i-2,j,k,l} - 8\phi_{i-1,j,k,l} + 8\phi_{i+1,j,k,l} - \phi_{i+2,j,k,l}}{12\Delta x} + O(\Delta x^4), \tag{7}$$

$$\left(\frac{\partial^2 \phi}{\partial x^2}\right)_{i,j,k,l} = \frac{-\phi_{i-2,j,k,l} + 16\phi_{i-1,j,k,l} - 30\phi_{i,j,k,l} - 16\phi_{i+1,j,k,l} - \phi_{i+2,j,k,l}}{12\Delta x^2} + O(\Delta x^4), \tag{8}$$

where Δx denotes the uniform spatial grid spacing in the x-direction.

As for the unsteady terms, i.e. in timewise direction, the following third-order backward FD scheme is employed.

$$\left(\frac{\partial \phi}{\partial t}\right)_{i,j,k,l} = \frac{11\phi_{i,j,k,l} - 18\phi_{i,j,k,l-1} + 9\phi_{i,j,k,l-2} - 2\phi_{i,j,k,l-3}}{6\Delta t} + O(\Delta t^3), \tag{9}$$

where Δt denotes the constant time step size.

In order to discretize the spatial boundary conditions, Saitoh [12] introduced the full fourth-order expressions with the virtual grid point as follows:

(i) Adiabatic condition

$$T_{i-1} = T_{i+1}; \quad T_i = \frac{48T_{i+1} - 36T_{i+2} + 16T_{i+3} - 3T_{i+4}}{25}. \tag{10}$$

(ii) Constant temperature condition and non-slip condition for velocity

$$T_i = C; \quad T_{i-1} = 2C - T_{i+1}, \tag{11}$$
$$u_i = 0; \quad u_{i-1} = -u_{i+1}. \tag{12}$$

(iii) Vorticity boundary conditions

$$\omega_i = (\nabla \times u)_i, \tag{13}$$
$$\omega_{i-1} = 5\omega_i - 10\omega_{i+1} + 10\omega_{i+2} - 5\omega_{i+3} + \omega_{i+4}. \tag{14}$$

As for the timewise boundary conditions, we simply set at $t = 0$ as follows:

$$T_{l=1} = C; \quad T_{l=0} = 2C - T_{l=2};$$
$$T_{l=-1} = 2T_{l=0} - T_{l=1}, \tag{15}$$

$$\omega_{l=1} = 0; \quad \omega_{l=0} = -\omega_{l=2}; \\ \omega_{l=-1} = 2\omega_{l=0} - \omega_{l=1}. \tag{16}$$

As the terminal boundary conditions, the assumption to be steady (i.e., $\frac{\partial T}{\partial t} = 0$) are not used in this paper because of use of the backward FD scheme as Eq. (9).

As an iterative solver for the TSM computations, we employed the ordinary SOR method and the solution was obtained in the time–space domain, i.e. the governing equations were solved point by point using successive correction procedures as noted in Section 2.

To explain the TSM formulation, we take the temperature equation as an example. After the TSM formulation, the semi-discrete form is obtained as follows:

$$T^{n+1}_{i,j,k,l} = T^{n}_{i,j,k,l} + \alpha\left(\frac{1}{PrRe}\nabla^2 T - \left(\frac{\partial T}{\partial t} + (u\cdot\nabla)T\right)\right)^{n}_{i,j,k,l}, \tag{17}$$

where n denotes the iteration number, and i, j, k and l indicate the grid indexes for the x-, y-, z- and t-directions. α is the acceleration parameter for iterations.

The convergence of computations is declared when the following convergence criterion, L2-mean of residuals (mean square root of error par grid point) for vorticity equations, are less than 10^{-6}. When this criterion is satisfied, the temperature and velocity-vector potential equations show further convergence of 1–2 orders of magnitude smaller than that of the vorticity equations.

4. Numerical results and discussion

4.1. Original and benchmark solutions

For the present range of Ra numbers, solutions were obtained on uniform meshes from $40\times40\times40\times10$, $80\times80\times80\times10$ and $120\times120\times120\times10$.

In this paper, the following characteristic quantities are presented.

$\phi_{2\text{center}}$	y-component of the vector potential at the center of the cavity
$\omega_{2\text{center}}$	y-component of the vorticity at the center of the cavity
$u_{1\ \max}$	maximum horizontal velocity for x-direction on center line ($x = 0.5, y = 0.5$) of the cavity and its location
$u_{3\ \max}$	maximum vertical velocity for z-direction on center line ($y = 0.5, z = 0.5$) of the cavity and its location
$Nu_{1/2}$	average Nusselt number on the vertical mid-plane ($x = 0.5$) of the cavity
Nu_{mean}	average Nusselt number on the vertical boundary ($x = 0$ or 1) of the cavity
S_{center}	stratification factor at the center of the cavity

Here, as for the x-direction, the local Nusselt number at each grid point is defined as

$$Nu_{\text{local}}(x,y,z) = PrRe\cdot u_1 T - \frac{\partial T}{\partial x}. \tag{18}$$

The average Nusselt number at the constant x-plane is defined as

$$Nu(x) = \int_0^1\int_0^1 \left(PrRe\cdot u_1 T - \frac{\partial T}{\partial x}\right)\mathrm{d}y\,\mathrm{d}z. \tag{19}$$

In order to integrate Eq. (19), the Simpson's rule was used.

The stratification factor S is defined as

$$S(x,y,z) = \frac{\partial T}{\partial z}. \tag{20}$$

In order to compute the temperature gradient, the fourth-order approximation to the $\partial T/\partial x$, which is consistent with the finite differentiation of the temperature equation, was always used except for on boundaries. As for the boundaries at $x = 0$ and 1, u was set as 0 and the temperature gradient was approximated by the fourth-order one-sided formula, from which the adiabatic condition (10) was introduced.

The computed results were time-asymptotic and converged to the steady state from initial isothermal and quiescent conditions. Although we tested the cases changing the time step size to be 1.0 or larger (e.g., O(10)), the temporally converged solutions were not affected by this.

A CPU time would take around 40 h for the $Ra = 10^6$ case. In this case, the acceleration parameter α for vorticity, velocity-vector potential and temperature equations are 0.2, 1.7 and 0.3 respectively and we used the finest $120\times120\times120\times10$ uniform grids with the time step size of 1.0 on the VT-Alpha600 Workstation with about a 120 Mflops computing speed.

For the three Ra numbers, the converged characteristic quantities in each grid and some reference values are compared and tabulated in Table 1. The locations for maximum velocities are calculated using the least square method. This method will have small errors as far as the sufficient grid resolutions are available.

In our results, the converged flow pattern and temperature distributions are symmetrical with respect to the center of the cavity for all cases. The validity of the TSM has already been confirmed in Refs. [10,11], hence the comparison with the conventional or explicit method were not shown for brevity.

In the case of $Ra = 10^4$, the solutions seemed to show a good convergence for the grid spacing on the $120\times120\times120$ grids, particularly in the $\omega_{2\,\text{center}}$ and S_{center}. As can be seen in Table 1, our results for $u_{1\ \max}$

Table 1
The original solutions at $Ra = 10^4$, 10^5 and 10^6

Ra	Grid size		$\phi_{2\,\mathrm{center}}$	$\omega_{2\,\mathrm{center}}$	$u_{1\,\max}$ (z)	$u_{3\,\max}$ (x)	$Nu_{1/2}$	Nu_{mean}	S_{center}
10^4	Present	0.025	0.05687	1.1034	0.1989 (0.8250)	0.2211 (0.1253)	2.0650	2.0814	0.8667
		0.0125	0.05507	1.1019	0.1985 (0.8250)	0.2218 (0.1125)	2.0638	2.0676	0.8636
		0.00833	0.05495	1.1018	0.1984 (0.8250)	0.2216 (0.1167)	2.0636	2.0634	0.8634
	Fusegi et al. [6]		–	–	0.2013 (0.8167)	0.2252 (0.1167)	–	2.100	
10^5	Present	0.025	0.03520	0.2831	0.1423 (0.8500)	0.2407 (0.0751)	4.4203	4.4309	1.1339
		0.0125	0.03418	0.2590	0.1418 (0.8500)	0.2450 (0.0625)	4.3834	4.3907	1.0904
		0.00833	0.03406	0.2576	0.1416 (0.8500)	0.2461 (0.0667)	4.3685	4.3713	1.0874
	Fusegi et al. [6]		–	–	0.1468 (0.8547)	0.2471 (0.0647)	–	4.361	–
10^6	Present	0.025	0.02141	0.1423	0.08129 (0.8500)	0.2382 (0.0500)	9.2209	9.4202	0.9880
		0.0125	0.01991	0.1369	0.08105 (0.8500)	0.2606 (0.0375)	8.8582	8.8681	0.9262
		0.00833	0.01979	0.1366	0.08110 (0.8583)	0.2587 (0.0333)	8.7757	8.7732	0.9192
	Le Peutrec et al. [5]		–	–	–	–	–	8.657	–
	Fusegi et al. [6]		–	–	0.08416 (0.8557)	0.2588 (0.0331)	–	8.770	–
	Janssen et al. [8]		–	–	0.08099	0.2585	–	8.6393	0.9103
	Haldenwang et al. [13]		–	–	–	–	–	8.61	0.9175

and $u_{3\,\max}$ are smaller than those by Fusegi et al. [6] within a 1.6% difference. The location of $u_{3\,\max}$ at the mid-plane of $y = 0.5$ is the same with their results. Hence, their results for a boundary layer thickness are very similar to our results. As for the case of $Ra = 10^5$, the dependence on the grid spacing exists, particularly for Nusselt numbers. This was due to the integration procedures. In this case, our results for $u_{1\,\max}$ and $u_{3\,\max}$ are also smaller than those by Fusegi et al. [6] within a 3.5% difference. As for the cases of $Ra = 10^6$, our results for $u_{1\,\max}$ and $u_{3\,\max}$ is in good agreements with the results by Janssen et al. [8]. They have conducted computations on the $120\times120\times120$ non-uniform grid using the second-order finite volume method.

Table 2 is the summary of the benchmark solutions based on the original solutions. The benchmark solutions were extrapolated from the two original solutions by using the following Richardson extrapolation:

$$X_t = \frac{X_1 - (\Delta_1/\Delta_2)^m X_2}{1 - (\Delta_1/\Delta_2)^m}. \tag{21}$$

Here, X_1 and X_2 are the original solutions for the grid spacing Δ_1 and Δ_2, respectively. X_t represents the extrapolated benchmark solutions. Also m is the order of discretization error and it was assumed to be 4 in this paper. As pointed out by de Vahl Davis [1], the order of accuracy at the local grid point is not always constant, varying until the grid spacing reaches zero. Therefore he had decided to use the original solutions on the finest two grids for extrapolation procedures and the order of accuracy m was considered to be the same with that of the discretization methods. In this paper, we followed their methodologies.

Fig. 3 shows the relationship between the grid spacing and the percentage error for some selected characteristic quantities. Solid lines are drawn by using the least square method. From these dependencies, the order of discretization error m is not constant but in the range of 3.3–5.2.

4.2. Characteristics of flow and heat transfer

In this section, only the results on the $120\times120\times120\times10$ grids are shown for explanation of

Table 2
Summary of the present benchmark solutions

Ra	$\phi_{2\,\mathrm{center}}$	$\omega_{2\,\mathrm{center}}$	$u_{1\,\max}\ (z)$	$u_{3\,\max}\ (x)$	$Nu_{1/2}$	Nu_{mean}	S_{center}
10^4	0.05492	1.1018	0.1984 (0.8250)	0.2216 (0.1177)	2.0636	2.0624	0.8634
10^5	0.03403	0.2573	0.1416 (0.8500)	0.2464 (0.0677)	4.3648	4.3665	1.0867
10^6	0.01976	0.1366	0.08111 (0.8603)	0.2583 (0.0323)	8.7097	8.6973	0.9175

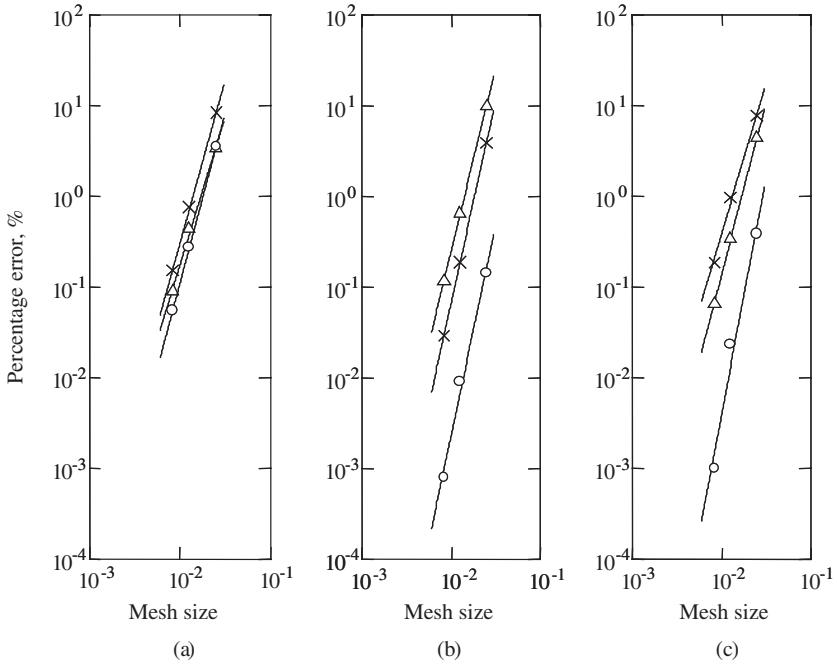

Fig. 3. Relative percentage error for (a) $\phi_{2\,\mathrm{center}}$, (b) $\omega_{2\,\mathrm{center}}$ and (c) S_{center} (○: $Ra = 10^4$, △: $Ra = 10^5$, ×: $Ra = 10^6$).

characteristics of flow and heat transfer in the cubic cavity.

Temperature T, vorticity ω_2 and vector potential ϕ_2 contours at the mid-plane of $y = 0.5$ of the cavity are shown in Fig. 4, where "0(0.1)1" in the caption means that the minimum contour is 0, the maximum contour is 1, and the contour increment is 0.1. The same goes for other captions. Fig. 5 shows the velocity distributions of u_1 and u_3 within the mid-plane of $y = 0.5$ of the cavity. These results are very favorable to those of the two-dimensional results [1–3,13,14]. As seen in the figures, the boundary layers near the vertical walls get thinner as the Rayleigh number increases. In contrast, the boundary layers near the upper and lower walls are not so thin as near the vertical walls.

In Fig. 6, the cross-sectional velocity contours of u_1 at $x = 0.5$ and u_3 at $z = 0.5$ are drawn. Contours with minus value are expressed by dashed lines. In the $Ra = 10^4$ case, the single point of the maximum (and minimum) u_1 is located at the mid-plane of $y = 0.5$. On the other hand, two peaks of u_1 appear near the corners for both the $Ra = 10^5$ and 10^6 cases. Those locations for $Ra = 10^6$ become closer to the edges retaining its symmetry for the mid-plane of $y = 0.5$ compared to those for $Ra = 10^5$. As for the u_3 contours, two peaks have already appeared in the $Ra = 10^4$ case. As the Rayleigh number increases, the peaks tend to move toward the corners. These results suggested that the spiral flow tubes were formed along the walls, and heat and mass transfer take place mainly in that flow tube.

Fig. 7 shows the local Nusselt numbers, defined in Eq. (16), of the vertical planes at $x = 0$, 0.5 and 1, respectively. The contours with minus values were also drawn in dashed lines. A similar behavior of the cross-sectional velocities for the locations of the maximum local Nusselt number was also seen. For the $Ra = 10^4$

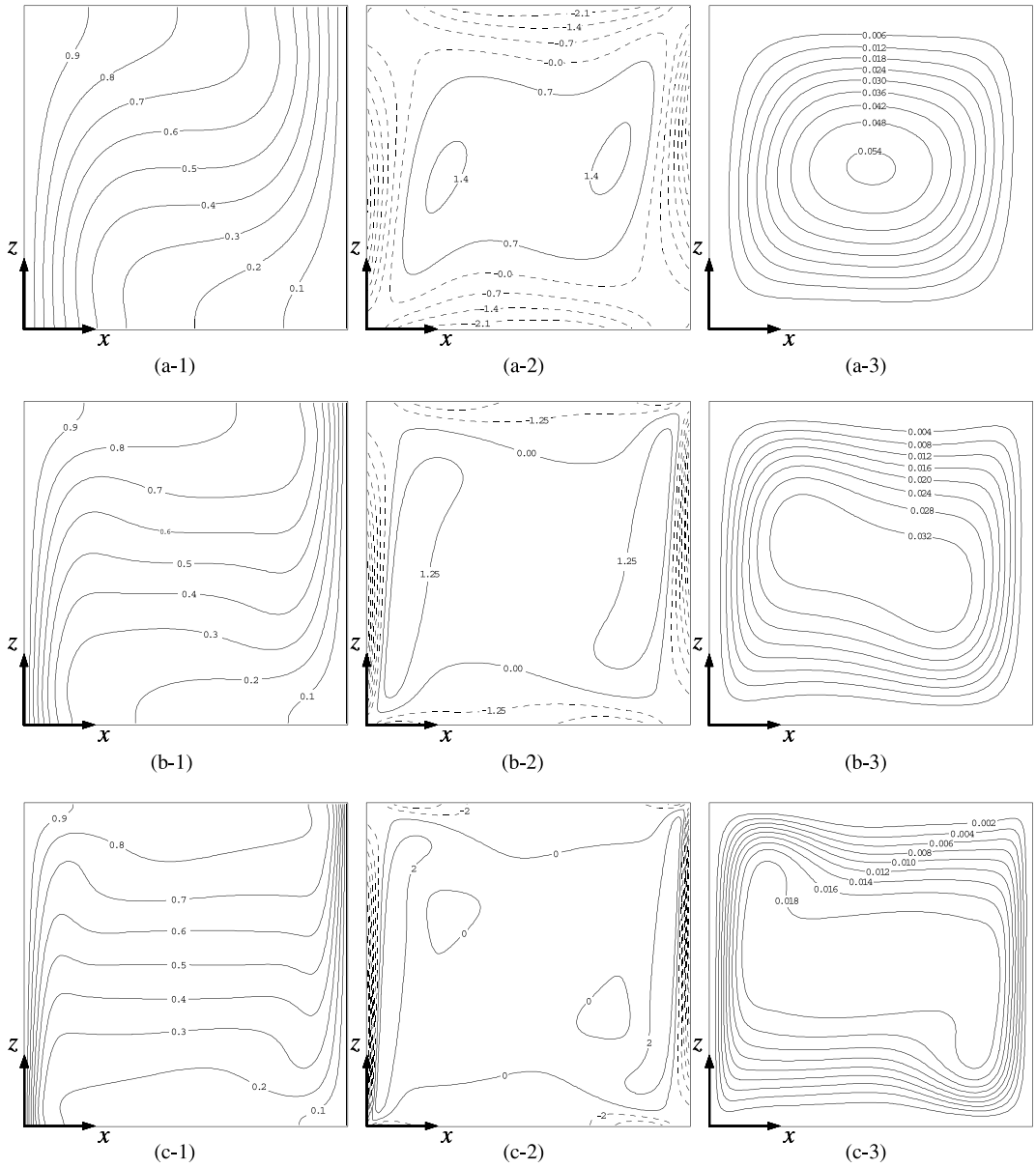

Fig. 4. Temperature, vorticity ω_2 and vector potential ϕ_2 at the mid-plane of $y = 0.5$. $Ra = 10^4$: (a-1) T contours at 0(0.1)1; (a-2) ω_2 contours at −4.9(0.7)1.4; (a-3) ϕ_2 contours at 0(0.006)0.054. $Ra = 10^5$: (b-1) T contours at 0(0.1)1; (b-2) ω_2 contours at −8.75(1.25)1.25; (b-3) ϕ_2 contours at 0(0.004)0.04. $Ra = 10^6$: (c-1) T contours at 0(0.1)1; (c-2) ω_2 contours at −16(2)2; (c-3) ϕ_2 contours at 0(0.002)0.018.

case, the peak is just located on the centerline of the cavity. In contrast, as the Rayleigh number increases, two peaks appear near the corners, but they are very weak and not clearly seen in the contours in Fig. 7(a-1)–(c-1) and (a-3)–(c-3). As for the mid-plane of $x = 0.5$ (Fig. 7(a-2)–(c-2)), two peaks also appear but their locations do not get closer to the sidewalls or edges as the Rayleigh number increases. The peaks that appeared seemed to be just getting sharpened. Figs. 7 and 6 indicate that the heat transfer across the mid-plane of $x = 0.5$ are mainly done by advection, in contrast to the area near the vertical boundaries.

5. Conclusions

In this paper, the new benchmark solutions for a natural convection in a cubical cavity has been presented

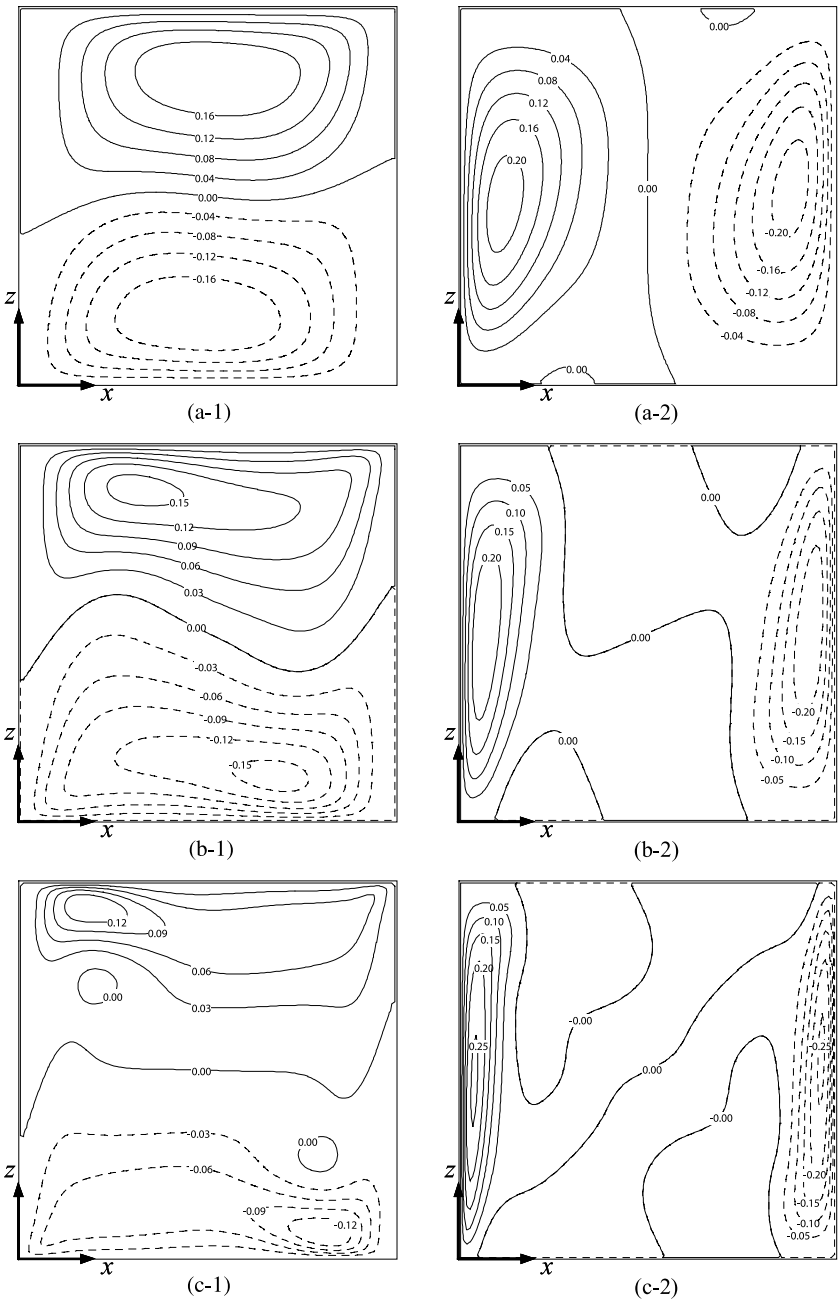

Fig. 5. The velocity contours of u_1 and u_3 at the mid-plane of $y = 0.5$. $Ra = 10^4$: (a-1) u_1 contours at $-0.16(0.04)0.16$; (a-2) u_3 contours at $-0.2(0.05)0.2$. $Ra = 10^5$: (b-1) u_1 contours at $-0.15(0.03)0.15$; (b-2) u_3 contours at $-0.2(0.05)0.2$. $Ra = 10^6$: (c-1) u_1 contours at $-0.15(0.03)0.15$; (c-2) u_3 contours at $-0.25(0.05)0.25$.

for $Ra = 10^4$, 10^5 and 10^6 with $Pr = 0.71$. The flow and heat transfer characteristics were also clarified.

The computations were efficiently performed using the fourth-order finite difference TSM, which is an efficient and fast numerical solver for general heat transfer and fluid flow problems.

The conclusions are summarized as follows:

(1) The computations were efficiently conducted using the TSM, and temporally converged solutions were obtained at the three Rayleigh numbers for $Ra = 10^4$, 10^5 and 10^6 with $Pr = 0.71$. The TSM can take a large

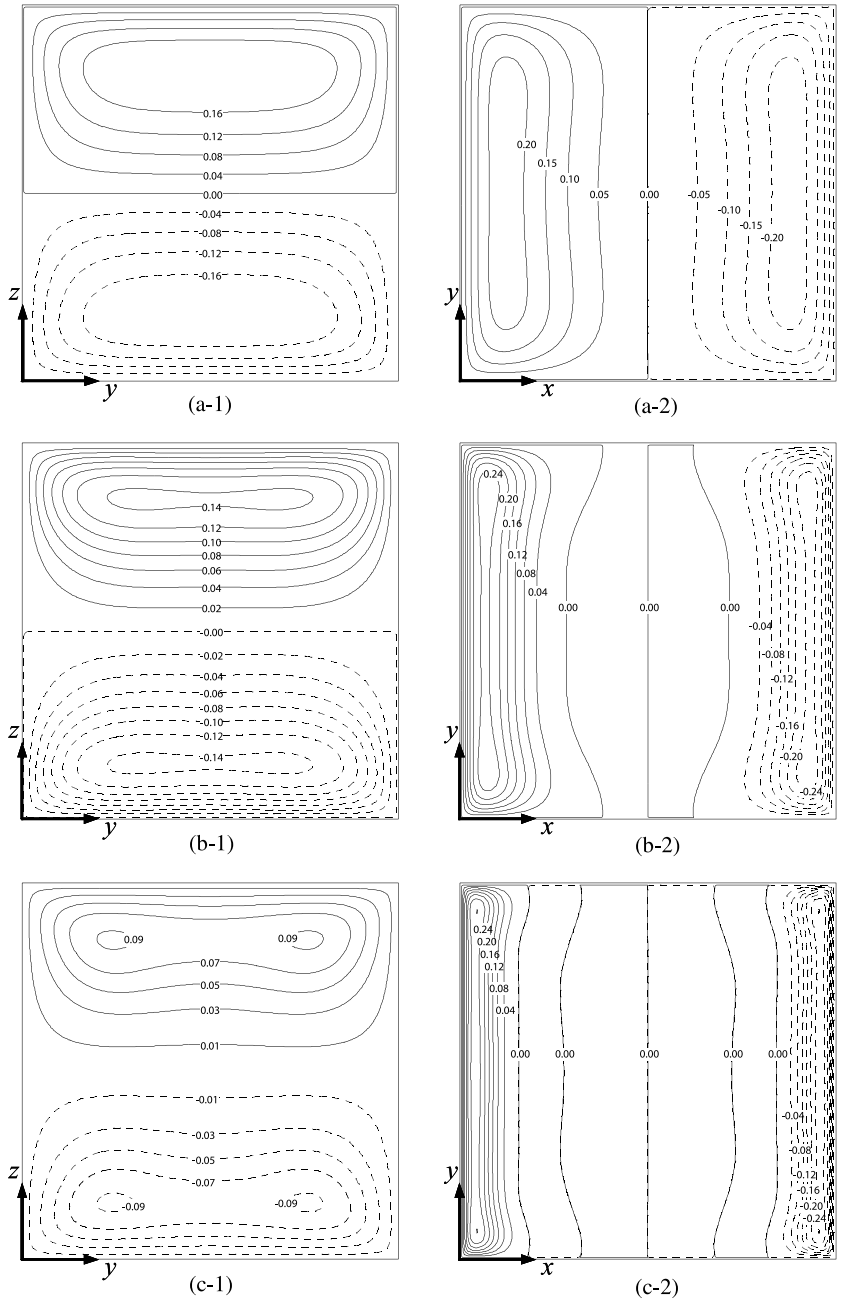

Fig. 6. Contours of the cross-sectional velocity vertical to the mid-planes of $x = 0.5$ (left) and $z = 0.5$ (right). $Ra = 10^4$: (a-1) u_1 contours at $-0.16(0.04)0.16$; (a-2) u_3 contours at $-0.2(0.05)0.2$. $Ra = 10^5$: (b-1) u_1 contours at $-0.14(0.02)0.14$; (b-2) u_3 contours at $-0.24(0.04)0.24$. $Ra = 10^6$: (c-1) u_1 contours at $-0.09(0.02)0.09$; (c-2) u_3 contours at $-0.28(0.04)0.28$.

time step arbitrarily to be an outstanding time-saving solver for the time-consuming problems such as the high Rayleigh number problems computed in this paper.

(2) The resulted benchmark solutions with the fourth-order of accuracy were obtained for a three-dimensional natural convection in a cubical cavity of Rayleigh numbers of the 10^4, 10^5, and 10^6 and a Prandtl number of 0.71. The orders of discretization errors for selected quantities are in the range of 3.3–5.2. The benchmark solutions will be useful for evaluation of any numerical methodologies for incompressible flows.

(3) The flow patterns and temperature distributions are presented. As for the mid-plane of $y = 0.5$, the results are very similar to those obtained in two-dimen-

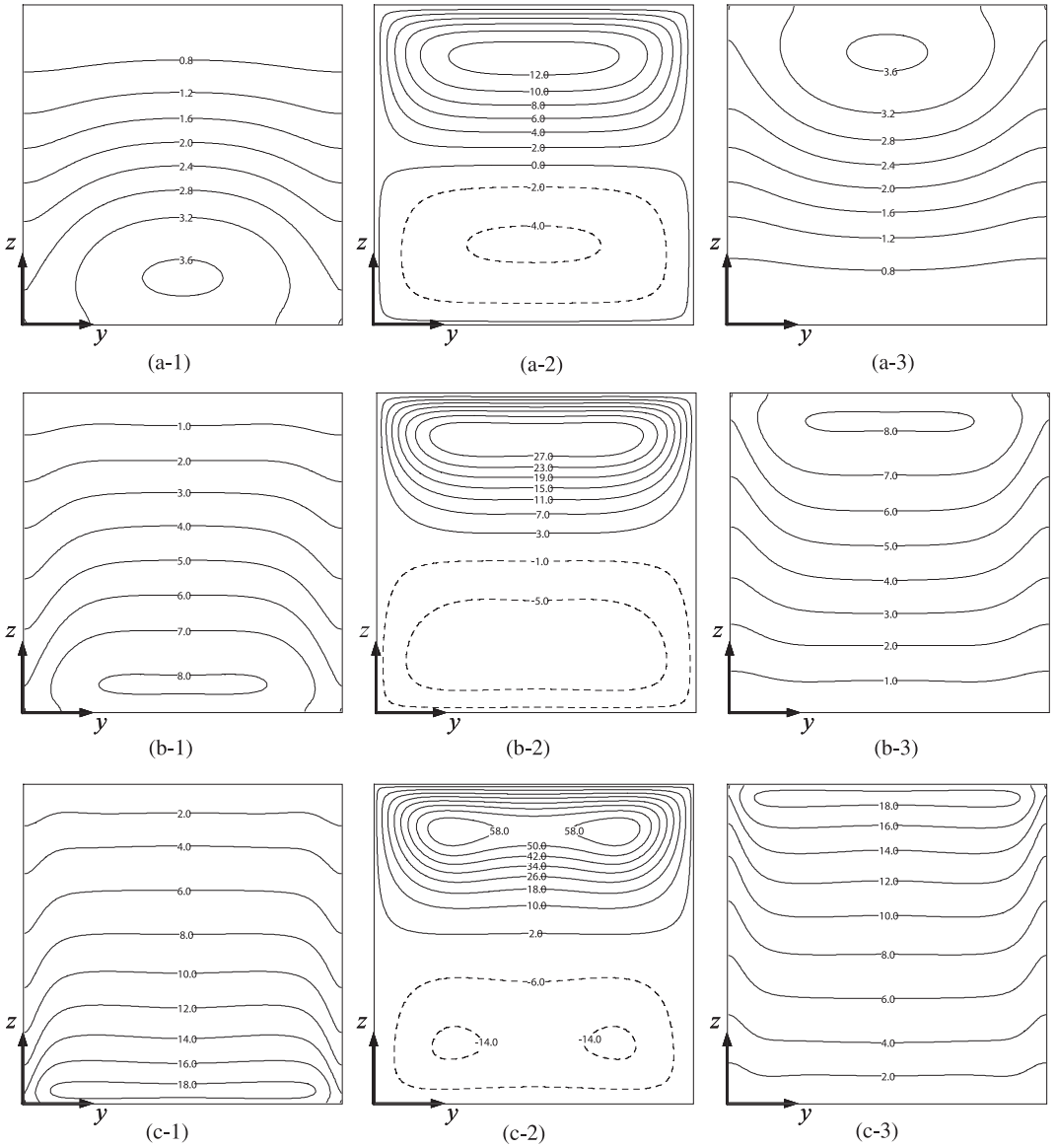

Fig. 7. The local *Nu* number distributions of the vertical planes at $x = 0$ (left), 0.5 (center) and 1 (right). $Ra = 10^4$: (a-1) contours at 0.8(0.4)3.6; (a-2) contours at −4(2)12; (a-3) contours at 0.8(0.4)3.6. $Ra = 10^5$: (b-1) contours at 1(1)8; (b-2) contours at −5(4)27; (b-3) contours at 1(1)8. $Ra = 10^6$: (c-1) contours at 2(2)18; (c-2) contours at −14(8)58; (c-3) contours at 2(2)18.

sions. As the planes of $z = 0.5$ or $x = 0.5$, the cross-sectional velocity contours show two peaks near the corners with the Rayleigh numbers of 10^5 and 10^6. In addition, the local Nusselt numbers on the isothermal boundaries also show two weak peaks.

References

[1] G. de Vahl Davis, Natural convection of air in a square cavity: a bench mark numerical solution, Int. J. Numer. Methods Fluids 3 (1983) 249–264.

[2] T.S. Saitoh, K. Hirose, High-accuracy bench mark solutions to natural convection in a square cavity, Comput. Mech. 4 (1989) 417–427.

[3] M. Hortmann, M. Peric, G. Scheuerer, Finite volume multigrid prediction of laminar natural convection: bench-mark solutions, Int. J. Numer. Methods Fluids 11 (1990) 189–207.

[4] G.D. Mallinson, G. de Vahl Davis, Three-dimensional natural convection in a box: a numerical study, J. Fluid Mech. 83 (1977) 1–31.

[5] Y.Le. Peutrec, G. Lauriat, Effects of the heat transfer at the side walls on natural convection in cavities, Trans. ASME J. Heat Transfer 112 (1990) 370–378.

[6] T. Fusegi, J.M. Hyun, K. Kuwahara, B. Farouk, A numerical study of three-dimensional natural convection in a differentially heated cubical enclosure, Int. J. Heat Mass Transfer 34 (1991) 1543–1557.
[7] S.M. Bilski, J.R. Lloyd, K.T. Yang, An experimental investigation of the laminar natural convection velocity in square and partitioned enclosures, in: Proceedings of the Eighth International Heat Transfer Conference, vol. 4, 1986, pp. 1513–1518.
[8] R.J.A. Janssen, R.A.W.M. Henkes, C.J. Hoogendoorn, Transition to time-periodicity of a natural-convection flow in a 3D differentially heated cavity, Int. J. Heat Mass Transfer 36 (1993) 2927–2940.
[9] W. Jia, Y. Nakamura, M. Yasuhara, Natural convection flow solver in primitive variable form, J. Jpn. Soc. Fluid Mech. 9 (1990) 34–52.
[10] T.S. Saitoh, M. Nakamura, High-efficiency numerical method for heat transfer problem including natural convection in a square cavity, in: Proceedings of the 28th National Heat Transfer Symposium in Japan, 1991, pp. 145–147.
[11] T.S. Saitoh, M. Nakamura, T. Gomi, Time–space method for multidimensional melting and freezing problems, Int. J. Numer. Methods Eng. 37 (1994) 1793–1805.
[12] T.S. Saitoh, Computer-Aided Heat Transfer, Yokendo Publ, Tokyo, 1989.
[13] P. Haldenwang, G. Labrosse, 2-D and 3-D spectral Chebyshev solutions for free convection at high Rayleigh number, in: Proceedings of the Sixth International Symposium on Finite Element Method in Flow Problems, 1986, pp. 261–266.
[14] H. Okanaga, T. Tanahashi, Numerical analysis of natural convection in a square cavity at high Rayleigh numbers using the GSMAC finite-element methods, Trans. Jpn. Soc. Mech. Eng. 56B-530 (1990) 2922–2929.